Alternative pyramid wavefront sensors

Maaike van Kooten
Jean Pierre Veran
Colin Bradley

Alternative pyramid wavefront sensors

Maaike van Kooten,a,b,* Jean Pierre Veran,a,c and Colin Bradleya
aUniversity of Victoria, Mechanical Engineering, Victoria, British Columbia, Canada
bLeiden Observatory, Leiden, Netherlands
cNRC-Herzberg, Victoria, British Columbia, Canada

Abstract. The feasibility of a lenslet-based pyramid wavefront sensor (L-PWFS) and a double roof prism-based PWFS (DR-PWFS) as alternatives to a classical PWFS are investigated in this work. Traditional PWFSs require shallow angles and strict apex tolerances, making them difficult to manufacture. Lenslet arrays and roof prisms, on the other hand, are both common optical components that can be used as a PWFS. Characterizing these alternative pyramids and understanding how they differ from a traditional pyramid will allow the PWFS to become more widely used. The sensitivity of the SUSS microOptics 300-4.7 array and two ios Optics roof prisms are compared with a double PWFS (D-PWFS), as well as the simulated performance of an idealized PWFS for varying amounts of modulation and induced wavefront error. In response to low-order Zernike modes, the L-PWFS shows much lower performance and quicker saturation for large amounts of wavefront errors. The DR-PWFS, on the other hand, performs as well as the D-PWFS for the tests conducted. We conclude from this that the DR-PWFS does provide a feasible alternative to the classical pyramid in a range of applications.

1 Introduction

The pyramid wavefront sensor (PWFS), proposed in 1996 as an alternative to the Shack–Hartmann wavefront sensor (SHWFS), has been shown to be more sensitive, yielding better performance for a given guide-star magnitude[1] and a significant gain in limiting magnitude[2] compared with the SHWFS. To create a PWFS, the optical device—a glass pyramid—is placed in the image plane of the system, with the spot focused on the pyramid's apex. The light is divided into four quadrants and imaged onto a detector located at the pupil plane. The pixels on the detector split the pupil into subapertures (done on all four images of the pupil) analogous to how each lenslet array splits the pupil in the SHWFS. As the light interacts with the edges of the pyramid, a modified knife edge test is performed. All four pupils are full images of the telescope aperture and encode information about the incoming wavefront.

Ragazzoni and Farinato[3] found that the PWFS has a significant signal-to-noise ratio (SNR) increase when operating in a closed-loop adaptive optics (AO) system compared with an SHWFS. Since the PWFS is limited by the diffraction of the telescope aperture, rather than the subaperture size as in the case for the SHWFS, an unmodulated PWFS is more sensitive than the SHWFS, leading to an increase in sky coverage for a natural guide star AO system.[1]

1.1 Difficulties with Pyramid Wavefront Sensors

The design specifications of a pyramid are relatively strict, requiring all four faces to have the same angle (to produce spots that are evenly spaced apart, minimizing calibrations and

desirable for an instrument such as NFIRAOS) and a good surface flatness. Most importantly, the edges need to be straight and narrow. This can be difficult for manufacturers due to the combination of the number of facets and the surface quality. Along with the low demand for pyramids and the current length of time needed to develop the necessary manufacturing techniques, it is not cost effective to implement in a laboratory setting for better understanding of these sensors and potentially even for on-sky applications (particularly for smaller telescopes).

Chromatic effects are also an issue for on-sky application of the PWFS as the sensing light usually spans a range of wavelengths. As light passes through the PWFS, the optical path traveled by each wavelength varies, which results in blurring and distortion of the pupil images. Although this work does not focus on the development of an achromatic PWFS, the behavior of each PWFS prototype studied in this work is briefly discussed in response to chromatic light. One possible achromatic PWFS is a reflective PWFS, which can either be created by a spatial light modulator[4] or a reflective pyramid element. Due to its achromatic properties, it has been important in developing an infrared PWFS;[5] however, it was not implemented as part of this work.

1.2 Outline

In this work, three different PWFS prototypes are implemented on an optical bench: a lenslet PWFS (L-PWFS), a double roof prism PWFS (DR-PWFS), and a double classic PWFS (D-PWFS). Their sensitivities for varying aberrations are investigated and compared, giving insight into their performance. Specifically, the amount of modulation is varied while the changes in sensitivity and the range for which the sensitivity is linear are compared with an idealized PWFS. Section 2 gives an

*Address all correspondence to: Maaike van Kooten, E-mail: vkooten@strw. leidenuniv.nl
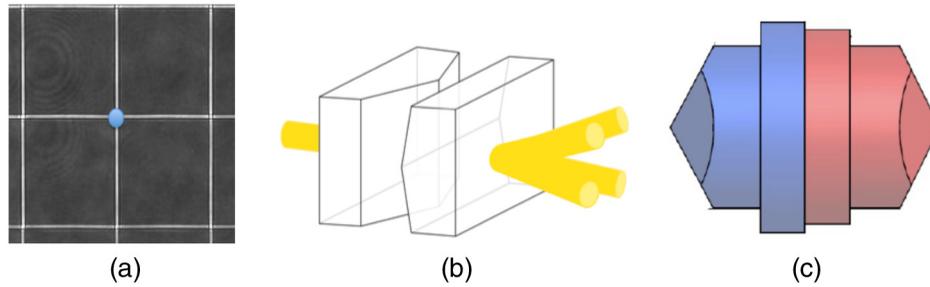
Fig. 1 Three different PWFSs tested in this work. (a) Lenslet array with a blue dot illustrating where the focal spot should hit the array to form a PWFS. (b) Schematic of a DR-PWFS. (c) The D-PWFS for the LBT, similar to the one used in this work.[7]

overview of the three PWFS. The methodology is outlined in Sec. 3. The results are presented in Sec. 4.

2 Pyramid Wavefront Sensor Prototypes

2.1 Lenslet Array Pyramid Wavefront Sensor

The Laboratory for Adaptive Optics at Santa Cruz first proposed the idea to implement a lenslet array as a PWFS.[6] A lenslet array is a grid of small lenses approximately a few hundred microns in pitch with focal lengths of a few millimeters. If the array is placed in the focal plane and the beam spot is placed at the intersection of four microlenses [see Fig. 1(a)], four pupils can be formed. This is optically equivalent to the pyramid as the boundary between microlenses provides a knife edge. Edge quality of the lenslet is analogous to apex/edge quality for a traditional pyramid and requires equivalent precision. The benefits of the lenslet are its ready availability, relatively low price, and constant improvement in quality by the manufacturers.

2.2 Double Roof Prism Pyramid Wavefront Sensor

By combining two roof prisms and aligning them such that their peaks point to each other but are aligned orthogonally [see Fig. 1(b)], the light will pass through the first prism, creating two beams that will each double as they pass through the second prism. The result is four pupil images each having passed through edge interfaces (roof angles), allowing for the knife edge test to be performed in both directions, creating a PWFS.

The sensitivity is preserved if the distance between the two roofs is smaller than the depth of focus and the focal plane sits exactly between the two roofs. In such a position, the symmetry of the pupils in x and y is preserved. If the prisms are separated more than the depth of focus, the beam is noticeably larger, which is equivalent to the loss of sensitivity when the apex of the pyramid is not in the focus (due to larger pupil spot size, similar to modulating the beam). Furthermore, an incorrect measurement of the phase would be made with the knife edge test when not in the focal plane.

An advantage of this design is that the prisms can be moved back and forth to get the best optical quality at the apex/edges. Roof prisms and similar prisms are also used in binoculars, making them easy to both buy off-the-shelf and order to specifications. Since the number of faces for one optical element is halved (compared with a classical pyramid), the strict tolerances (see Table 1 for the specifications for the roof prism used in this work) can also be more easily met by manufacturers, resulting in better tip quality and smaller edges.

Table 1 Specifications for roof prisms. Information from SCExAO provided via email correspondence.

Specification	Values
Width	25 ± 0.1 mm
Height	25 ± 0.1 mm
Thickness	10 ± 0.1 mm
Edge thickness	20 μm[8]
Scratch-Dig	40/20
Flatness	$\lambda/4$
Roof angle (fused silica at 700 nm)	3.775 deg $\pm 5'$

2.3 Double Pyramid Wavefront Sensor

The D-PWFS uses two glass pyramids glued back-to-back such that the beam enters the four-facet side and leaves through a four-facet side [as shown in Fig. 1(c)]. This relaxes the angle tolerances[9] and allows for the best match between two pyramids to be found for optimal performance. They are made from different materials, so the second pyramid corrects for the chromatic aberration from the first pyramid. This is done by carefully choosing the indices of refraction for the two pyramids. Note that, while the DR-PWFS is also constructed of two components, they must be of the same material to ensure symmetry in the x- and y-directions. A total of four prisms (two DR-PWFS) would be needed to make a similarly achromatic sensor.

3 Methods

The three PWFS prototypes: SUSS microOpitcs 300-4.7 lenslet array (which was chosen due to its superior edges compared with the other available arrays at the time of this work), two iosOptics roof prisms as a DR-PWFS (provided by the SCExAO team, see Table 1), and a D-PWFS (from Arcetri Observatory) were tested on the wavefront sensing bench at NRC-Herzberg. The PWFS optical path consisted of a fast steering mirror (FSM) to perform modulation, an imaging lens, a PWFS optical element, a reimaging lens, and a camera (see Fig. 2, pink path). Due to the specifications of each PWFS, two different cameras were used: a PointGrey Flea3 (for the D-PWFS only) and a PointGrey Grasshopper. For each PWFS, the lenses before and after the PWFS were changed (different focal lengths) along with the camera position. The modulation
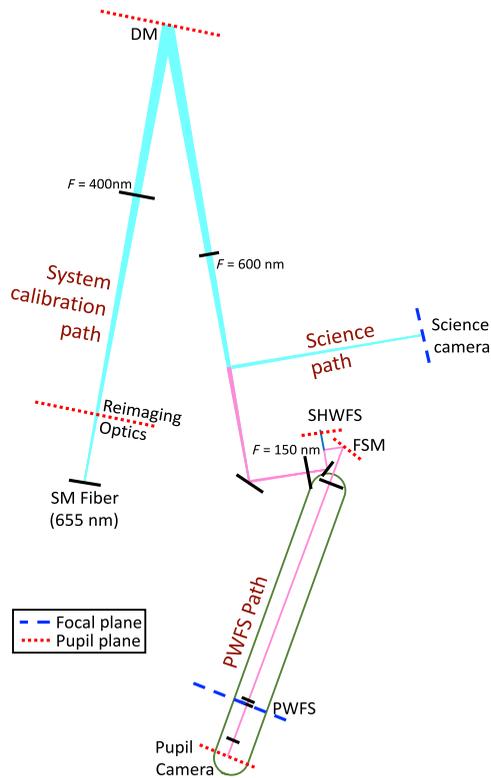
Fig. 2 Schematic of wavefront sensing bench containing a PWFS and an SHWFS. The green box indicates the elements that are changed for each of the three PWFS.

radii were calibrated by first placing a camera in the focal plane of the PWFS and then determining the FSM step size and offset angle. Then the camera was replaced with the PWFS. A beam-splitter was added before the PWFS focal plane to allow the camera (the PWFS focal spot camera) to be moved to another focal plane allowing for the focal spot's position and quality to be monitored. Since the synchronization of the modulation of the PWFS to the camera exposure is quite difficult, a step-by-step modulation approach was taken. An exposure was taken at 60 points (120 points for large modulation radii) along the modulation path. These images were then stacked to create one full modulation image.

Aligning the PWFS was the most important step in the experimental setup, with different methods required for aligning the different types of PWFS. For the L-PWFS, the alignment was iterative, with the pupil camera after the array being placed in a focal plane and array/camera system moved until the spots were focused on the detector. Then the camera was moved back into the pupil plane. For the DR-PWFS and the D-PWFS, the focal plane was found using a camera, and then the PWFS was placed at that focal plane. Small amounts of tilt were then introduced, and the amount of tilt needed to move all the light into two pupils was monitored. The PWFS system was iteratively moved until the minimum amount of tilt was found, indicating that the PWFS was in the focal plane. Further detail on the experimental setup is given in van Kooten et al.[8]

Non-common-path aberrations (NCPA) were minimized by running the PWFS in a closed loop. This was possible due to the deformable mirror (DM) being first controlled by the HASO2 SHWFS, which removed large aberrations, and then the residual errors were assumed to be within the linear regime of the PWFS.

The point-spread-function before the PWFS was monitored by the PWFS focal spot camera.

For each PWFS, three Zernike modes (tilt, astigmatism, and coma) were injected into the system via the FSM and DM, respectively, with increasing positive wavefront error. The DM injected error into the system through a closed loop operation with the SHWFS. The experiment was run for various modulation radii, and the PWFS sensitivity[9] [Eq. (1)] was calculated for each combination. In all cases, the pupils were oversampled at 64 pixels and larger. The minimum sampling for the DM-97 was 22 pixels (2×11 actuators across the pupil). The experimental data were later binned, so all pyramid measurements had the same sampling. The sensitivity of the prototypes was compared with an idealized PWFS modeled in the MATLAB toolbox OOMAO.[10] An idealized PWFS is defined, for this work, as a classical PWFS that is perfectly aligned with no edge or surface defects and an infinitely narrow edge, so it can be modeled simply as a phase mask in the Fourier domain. For the DR- and D-PWFS, sine waves were also produced on the DM, giving insight into the sensors' behaviors at higher spatial frequencies. The OOMAO pupil in the simulation was sampled by 23 pixels (actual number of slopes available and used in the calculation) but was binned automatically by the code for display purposes.

The PWFS sensitivity response (SR) is defined as

$$\mathrm{SR} = \sqrt{\frac{\sum_{i=1}^{2N} (S_i)^2}{2N}}, \tag{1}$$

where S_i is the calculated slope and N is the number of pixels in one pupil image. Note that the total number of slopes is $2N$, with both an x-slope and a y-slope calculated in each pixel of a pupil image. This defines the sensitivity of the PWFS as the root-mean-square (RMS) of the slope vector. Assuming noise affects each pixel independently, the sensitivity defined by Eq. (1) is directly proportional to the SNR of the measurement. SR curves for a given modulation radius are defined as the PWFS sensitivity as a function of incoming RMS wavefront error. They are normalized to the saturation value.

4 Results: Comparison of Pyramid Wavefront Sensors

In theory, a lenslet array provides a simple, flexible solution to the lack of available pyramids, with the performance and usefulness only limited by the intersection width. Overall, the lenslet array used here failed to produce a clear image of the pupil plane; see Fig. 3. When compared with the modeled PWFS, the pupil shape is not uniform and it appears to saturate quicker than expected. Before selecting the lenslet array, seven different lenslet arrays from various manufacturers were visually inspected (under a microscope) and the best array was chosen. However, with the poor pupil quality of the lenslet array chosen, further inspection of the selected lenslet's edges showed a width of 3% (8 to 9 μm), rather than 1% as stated by manufacturing standards. This difference could have caused the poor pupil quality seen, along with the inconsistent edges (not straight), nonorthogonal intersections, nonuniform grid (not square), inconsistent shape of the lenslets, and alignment errors. Figure 4 shows the tilt sensitivities of the L-PWFS (dashed curves) with the OOMAO PWFS sensitivities as a reference point (solid curves). As expected for no modulation (blue dashed line), the response was less than the model, indicating that the lenslet was
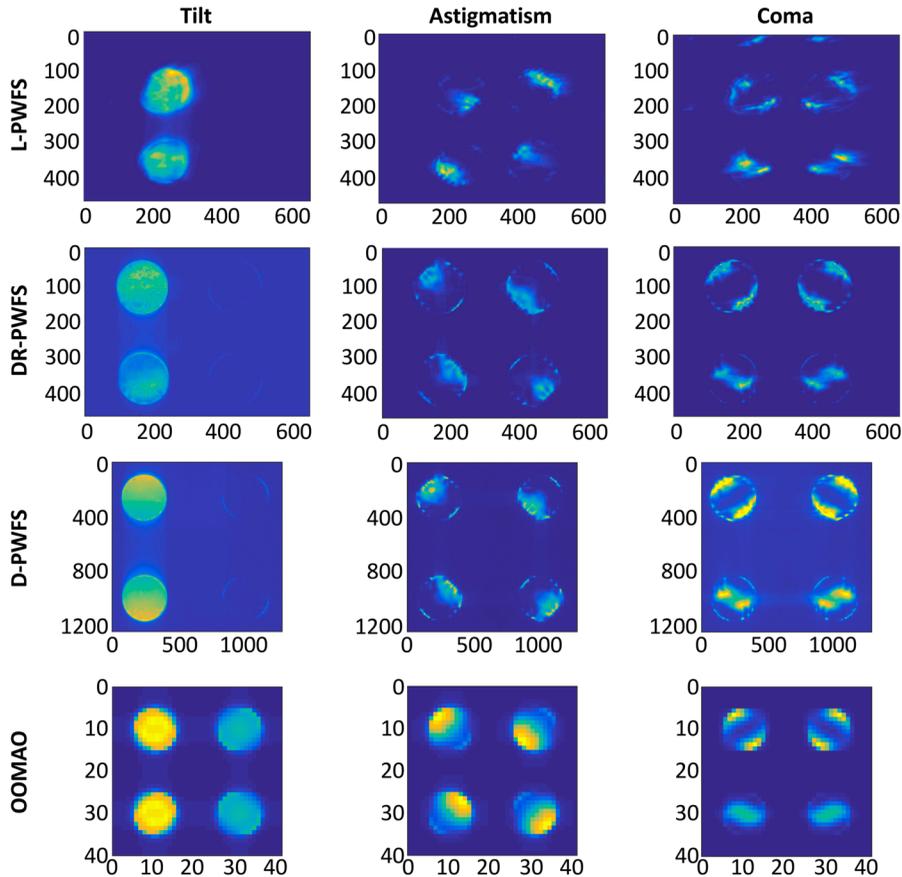
Fig. 3 PWFS pupils for three Zernike modes with a 100-nm RMS wavefront error and a modulation radius of $2\lambda/D$. Note that the D-PWFS pupil was imaged using a different camera than the other L- and DR-PWFS. This is indicated by the x and y axes, which show the camera pixels.

not as sensitive as an idealized PWFS. As the modulation radius was increased to $2\lambda/D$, the sensitivity began to match the theoretical sensitivity of no modulation. Once the sensitivity saturated, it stayed constant and then began to decrease due to light entering into the next set of pupils, degrading the measurement. For increasing modulation amplitude, there is no significant gain in the dynamic range (the cut-off frequency does not increase). For coma (top right of Fig. 4), the spot was large enough that modulation had no effect, and the wavefront sensor was already operating in the saturated regime. This grouping of the curves is expected for an idealized pyramid at much higher modes (Zernike mode 21 in simulation), indicating that the lenslet edge quality is very poor. The quality of the $10\lambda/D$ measurements were not good for astigmatism and coma and therefore not shown in Fig. 4.

It is important to note that, when interpreting Fig. 4, it is necessary to look at the combined behavior of the PWFS SR and the cut-off frequency (where the PWFS sensitivity is no longer linear). As the cut-off frequency increases, therefore increasing the range for which the sensitivity is linear, i.e., the dynamic range, the PWFS sensitivity decreases. Therefore, for an increase in dynamic range, sensitivity of the PWFS must be sacrificed. Moreover, from the model, it can be seen that the largest gain in range is expected for small modulation radii. This results in the largest discrepancy in the model and experimental data being for low modulation radii, where edge defects and misalignment would be amplified (see Sec. 3 for discussion on alignment).

The DR-PWFS showed better agreement with the model for tilt (see Fig. 4). Zero modulation had the same behavior as the theoretical prediction; for increasing modulation, the sensitivity curves were smooth, with the dynamic range increasing and the sensitivity decreasing. The increase in dynamic range for a given modulation was less than expected. At a modulation of $10\lambda/D$ for the DR-PWFS, the sensitivity matched the sensitivity and range for the theoretical modulation of $5\lambda/D$ (not shown in Fig. 4). Responses for astigmatism and coma (Fig. 4) showed a dramatic decrease overall in sensitivity compared with the model. This was the case both with and without modulation. The results indicate that, for lower modulation, larger dynamic ranges and less sensitivity were seen, until a turning modulation where the dynamic range became less than theory and sensitivity became greater than theory.

The pupils produced by the D-PWFS for tilt, astigmatism, and coma were extremely clear (Fig. 3) and showed good agreement with the theoretical PWFS pupils. The sensitivity curves for the three Zernike modes were not as smooth as expected, with a sharp turning point for astigmatism and coma. The sensitivities for tilt (Fig. 4) were as expected: no modulation was slightly less sensitive than OOMAO while for larger modulations the experimental data had greater sensitivity (the modulation does not provide the theoretical gain in dynamic range). This indicates that the amount of range gained and sensitivity lost was less than predicted by theory. For astigmatism, some of the sensitivities were still larger than predicted for higher
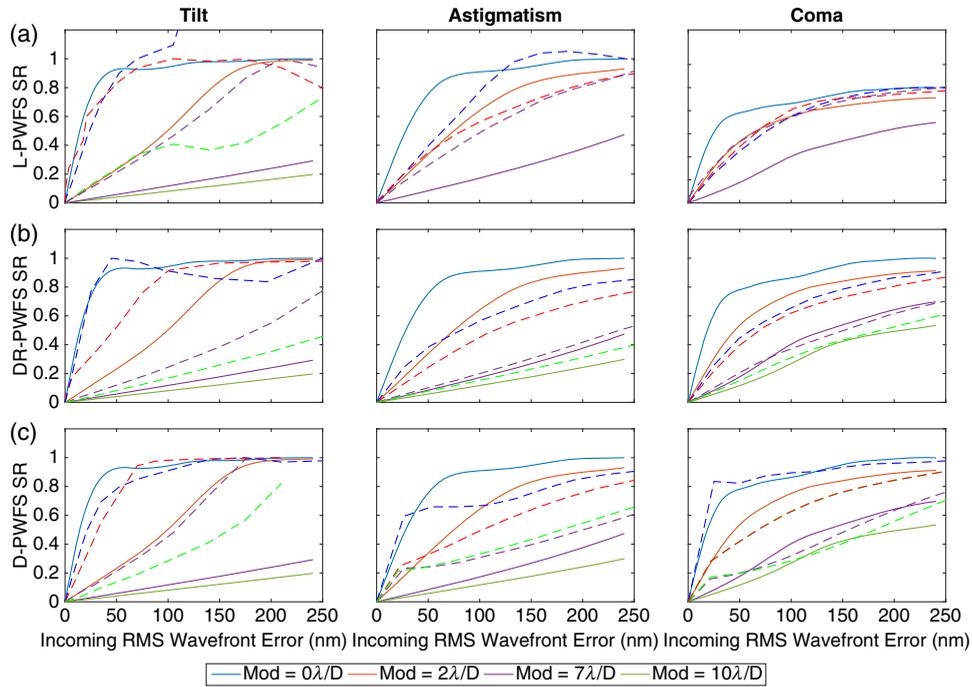
Fig. 4 Idealized PWFS SR curves (solid) for three Zernike modes with varying modulation along with the experimental data shown by the dashed lines. (a) L-PWFS, (b) DR-PWFS, (c) D-PWFS. The dynamic range refers to the range for which the PWFS is linear.

modulation. Only for coma were the sensitivities (for modulated cases) all less than predicted using OOMAO, suggesting that the modulation amplitude could be larger than thought. The differences in sensitivity between the idealized pyramid and the experimental results were most likely due to impure modes from NCPA between the SHWFS and PWFS and fitting errors on the DM; however, there is not a straightforward way to confirm this as there was no method to determine the amount of NCPA for the bench. These were minimized as best as possible by closing the loop between the PWFS and the DM with no modulation, starting from the best flat commands for the SHWFS. However, when a small amount of defocus, astigmatism, trefoil, and higher order modes are not accounted for, the input wavefront error is larger than expected. Since the pyramid wavefront sensor signal is defined as the RMS of the slope vector, the pyramid signal is larger for the same injected error. Using Fig. 4, for a given tilt curve, the difference between the theoretical and experimental curve is similar to adding a small amount of astigmatism (a higher order mode than is corrected) to the signal. The astigmatism curves show that the pyramid is extremely sensitive for small amounts and therefore has an effect on the performance. At higher modulations, the PWFS is less sensitive to these small aberrations as they are blurred out by the modulation pattern. Combining this with the effects of the optical element of the pyramid (e.g., the poor edge quality of the lenslet), and the DM fitting error, much of the difference between the theoretical and experimental curves can be explained.

These results show the L-PWFS to have the worst behavior due to the optical quality of the lenslet array itself. Larger modulation radii do not gain a lot of dynamic range for tilt and astigmatism while it does not gain any range for coma. The pitch of the lenslet limits the maximum modulation radius as well. Since the intersection width is a percentage of pitch, increasing the size of the lenslet does not solve this issue. However, it was

not clear from testing the low order Zernike modes which of the DR- and D-PWFS performed better. Hence, more experimental data were taken for high spatial frequencies.

Sine waves were produced, using the DM, to investigate the latter two PWFSs, as shown in Fig. 5. For a sine wave with amplitude of 100 nm, the pupils were binned along 45 deg creating a single sinusoidal wave [Figs. 5(a) and 5(b)]. The contrast (difference between the maximum and minimum values) for the DR-PWFS was larger than the D-PWFS with the minimum contrast for four cycles-per-aperture (cpa) being 0.4103 and 0.5393, respectively. The maximum contrast for the D-PWFS was still less than the DR-PWFS minimum. The contrast indicates how close the sensor was to saturation, suggesting that the D-PWFS could be closer to saturation at 100 nm than the DR-PWFS. However, the noise level of the different cameras along with any misalignment (pyramid not sitting exactly at the focus) prevents any concrete conclusions about which performs better from being made. Instead, the sine wave contrasts suggest that the DR-PWFS behaves at least as well as, and in a similar fashion to, the D-PWFS and can indeed be used as a PWFS.

To fully understand the behavior of the prototype sensors in detail, especially for higher order modes and for combinations of modes, additional measurements of the PWFS SR would be useful, along with modeling of the specific pyramid elements. However, this is outside the scope of this work.

5 Conclusion

The experimental testing of the three PWFS prototypes revealed key differences. Both the DR-PWFS and D-PWFS performed better than the L-PWFS in basic testing of the elements with low-order Zernike modes. This is due to the edge quality (uniformity) and thickness of the L-PWFS. Given that the slopes are encoded into the pupils using a knife edge test, the larger the edge, the less sensitivity as larger edges act as low pass filters. The measured thickness of the lenslet edge was larger than
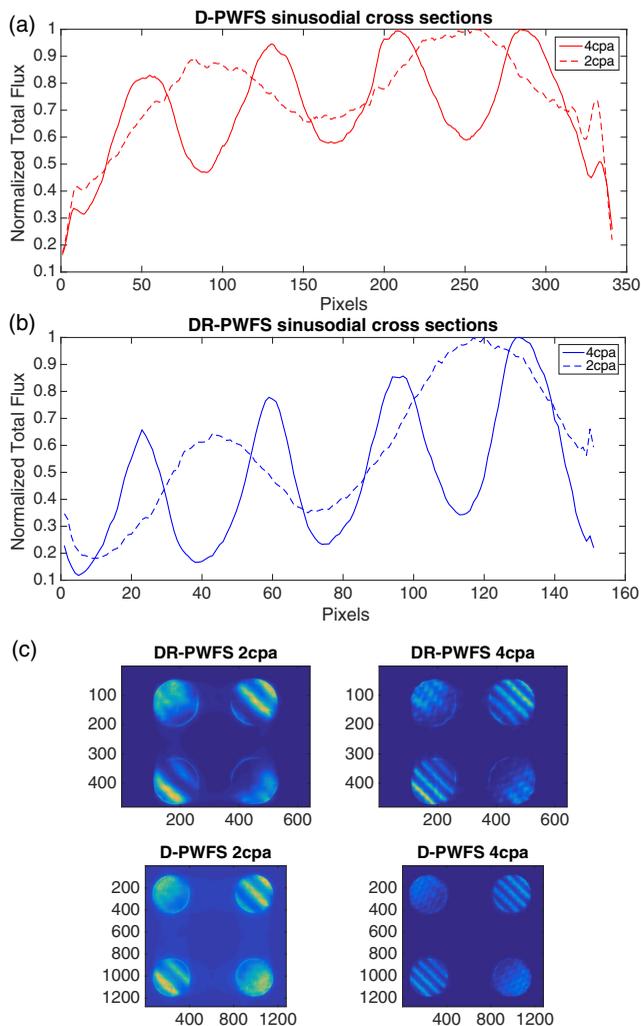
(a)

(b)

(c)

Fig. 5 (a) DR-PWFS summed cross section. (b) D-PWFS summed cross section. (c) DR- and D-PWFS pupils for 2 cpa and 4 cpa sine waves.

expected, as the standard method to fabricate these arrays does not focus on maximizing the fill factor necessarily (fill factor for SUSS Optics is not stated in catalogs) and often scales with pitch. More sophisticated fabrication techniques can be used to create better L-PWFS but at the tradeoff of cost and lack of availability.

More experimental data revealed that the DR-PWFS and D-PWFS are very similar in performance. This work shows

that the DR-PWFS is indeed a viable alternative to the classical PWFS, and the tests performed for these experimental setups show no dramatic differences in performance for a monochromatic source.

The DR- and D-PWFS will continue to be used and studied in a laboratory setting at NRC-Herzberg[9] on the Herzberg NFIRAOS Optical Simulator (HeNOS).[9] Efforts toward designing an achromatic DR-PWFS are also already under way.

References

1. C. Verinaud, "On the nature of measurements provided by a pyramid wave-front sensor," *Opt. Commun.* **233**, 27–38 (2004).
2. S. Esposito and A. Riccardi, "Pyramid wavefront sensor behavior in partial correction adaptive optics system," *Astron. Astrophys.* **369**, L9–L12 (2001).
3. R. Ragazzoni and J. Farinato, "Sensitivity of a pyramidic wave front sensor in closed loop adaptive optics," *Astron. Astrophys.* **350**(8), L23–L26 (1999).
4. V. Akondi, S. Castillo, and B. Vohnsen, "Digital pyramid wavefront sensor with tunable modulation," *Opt. Express* **21**(15), 18261–18272 (2013).
5. M. Feldt et al., "SUPY: an infrared pyramid wavefront sensor for Subaru," *Proc. SPIE* **6272**, 62722A (2006).
6. J. A. Johnson et al., "Pyramid wavefront sensing: theory and component technology development at LAO," *Proc. SPIE* **6272**, 62724R (2006).
7. A. Tozzi et al., "The double pyramid wavefront sensor for LBT," *Proc. SPIE* **7015**, 701558 (2008).
8. M. van Kooten et al., "Fast modulation and dithering on a pyramid wavefront sensor bench," *Proc. SPIE* **9909**, 99096G (2016).
9. E. Mieda et al., "Testing the pyramid truth wavefront sensor for NFIRAOS in the lab," *Proc. SPIE* **9909**, 99091J (2016).
10. R. Conan and C. Correia, "Object-oriented Matlab adaptive optics toolbox," *Proc. SPIE* **9148**, 91486C (2014).

Maaike van Kooten is currently a PhD candidate at Leiden Observatory studying adaptive optics with a focus on control theory. She completed her master's degree of applied science in mechanical engineering in 2016 and her bachelor's degree in physics and astronomy in 2014 both at the University of Victoria.

Jean Pierre Veran has contributed to a variety of adaptive optics projects including the Gemini Altair, TMT NFIRAOS, and Gemini GPI while working at NRC-Herzberg. As an adjunct professor at the University of Victoria, he helps supervise graduate students working in adaptive optics. He received his PhD from École Nationale Superieure des Télécommunications for his breakthrough work in point-spread-function reconstruction.

Colin Bradley is a professor at the University of Victoria in mechanical engineering. His research focuses on optical instrumentation for both astronomical instrumentation and ocean technology. Most recently his team built the RAVEN instrument, a multiobject adaptive optics system, which successfully demonstrated this new technology on the Subaru Telescope.